Lund University
Division of Synchrotron Radiation
Department of Physics

Sugar-Assisted Transfer Printing of K -Type Thin Film Strain Gauges onto Stainless Steel

LUNDS UNIVERSITET

Bachelor of Science Project in Physics
15 credits

Author: Yash Velaveti

Supervisor: Anders Mikkelsen

Co-supervisor: Ajsa Cuprija

Semester: Spring Semester 2026

Abstract

The integration of thin-film sensors onto geometrically complex industrial surfaces requires the transfer of microfabricated structures from flat donor substrates to non-planar receivers, a challenge that conventional elastomeric stamp methods cannot address at high curvature or surface roughness. This project investigates the REFLEX sugar-assisted transfer printing process as a route for integrating microfabricated K-type thin-film strain gauge structures, consisting of patterned Chromel (K+) and Alumel (K−) alloy poles on a nickel adhesion layer, onto polished stainless steel substrates. Two donor chip variants were produced, differing in whether the nickel adhesion layer was exposed to air between deposition steps, and subjected to the full REFLEX process including sugar coating, baking, liftoff, reflow, and dissolution. Selective retrieval of the Alumel (K−) poles was demonstrated for the air-exposed variant and attributed to oxide-mediated adhesion asymmetry arising from Cr_2O_3 formation at the Chromel/NiO interface. Eliminating the vacuum break in the second variant resolved this asymmetry but introduced thermally induced warping of the Chromel poles during baking, which was found to be governed by the peak baking temperature rather than the heating ramp rate. Successful transfer of geometrically intact Alumel poles onto the stainless steel receiver was observed by optical microscopy, and EDS elemental mapping confirmed full retrieval of the film stack in the second variant, consistent with a cleaner and less adhesive Ni/silicon interface in the absence of a vacuum break. The results demonstrate proof of concept for REFLEX transfer of K-type thin film structures onto stainless steel, while the challenge remains to identify baking techniques and temperature optimizations which achieve the complete transfer of the full sensor geometry.

Keywords: transfer printing, REFLEX, sugar carrier, thin-film strain gauge, K-type thermocouple, stainless steel, microfabrication, LundNanoLab.

Contents

List of Abbreviations

SEM Scanning Electron Microscopy

AFM Atomic Force Microscopy

REFLEX REflow-driven Flexible Transfer

PDMS Polydimethylsiloxane

PVD Physical Vapour Deposition

IPA Isopropyl Alcohol

1 Introduction

1.1 Background and Motivation

Accurate measurement of temperature and mechanical strain on surfaces is a recurring challenge in industrial and engineering applications. In processes such as metal cutting, pipeline monitoring, and turbine operation, surface conditions directly influence performance and lifetime, yet conventional sensors struggle to meet the demands of these environments[1]. Commonly used bulk wire thermocouples and bonded foil strain gauges introduce thermal mass that distorts local measurements, rely on adhesive layers that degrade under thermal stress, and cannot conform to curved or geometrically complex surfaces without compromising accuracy [2, 3].

Thin film sensors presents itself as a compelling alternative. The main advantage is the reduction of the thickness to micrometre levels and the ability to deposit it directly onto surfaces. As a result, issues with the adhesive interface and thermal mass are averted [3]. Sputtered thin-film strain gauges have been shown to match the accuracy of classical foil gauges while offering higher resistance values on smaller surfaces and removing adhesive creep as a source of drift [3]. However, the limitation is that the current photolithography and physical vapor deposition (PVD) techniques used to fabricate such sensors require flat and rigid substrates [4, 5]. Industrial surfaces tend to be more complex, often exhibiting inherent roughness and geometries such as tubes, corrugated plates, or curved components found in heat exchangers and fibre composite structures.

Transfer printing resolves this by adding an additional step before integration on target surfaces. In this new sequence, microstructures are first produced on a flat donor substrate under ideal cleanroom conditions, then physically relocated to a receiver of arbitrary geometry via a carrier medium [5]. Elastomeric PDMS stamps are carriers that work well on gently curved surfaces, but cannot stretch enough to accommodate the area changes that arise on tightly curved or complex geometries [4, 6]. The *Reflow-Enabled Film Transfer and Lamination onto Extreme surfaces* (REFLEX) process, introduced by Zabow [4] addresses this using a thermally reflowable sugar mixture as the carrier. Upon gentle heating the sugar with an embedded sensor melts and conforms to the shape of the receiver surface, and is later dissolved by water leaving no residue. This project applies the REFLEX method to transfer microfabricated K-type thin-film strain gauges, composed of Chromel (K+) and Alumel (K−) alloy legs joined at a sensing junction onto stainless steel substrates, a combination not previously demonstrated in the literature.

Stainless steel is ubiquitous in industrial settings, from chemical processing pipelines and heat exchangers to precision cutting tools and more. These components are operated under stressful conditions, where surface temperature and strain are the key quantities to maintain performance, combat wear, and prevent failure. Integrating sensors to measure such quantities directly on the surfaces of tools and machinery would enable seamless process monitoring guidelines and detection of component degradation [1, 2].

Recently, the direct sputter deposition of thin-film sensors onto stainless steel surfaces has been demonstrated by Dalelkhan et al. [1], who fabricated K-type thin-film thermocouples on 316 L substrates achieving sensitivities of $41.14\,\mu\mathrm{V}/^{\circ}\mathrm{C}$ and response times 71 % shorter than conventional wire sensors. However, direct deposition requires the target component to be placed inside the deposition chamber, which is impractical for components that are large, geometrically complex, or already installed. Transfer printing removes this constraint by decoupling fabrication from the target substrate entirely [4, 5].

1.2 Aim of the Project

The aim of this project is to investigate the feasibility of sugar-assisted REFLEX transfer printing as a method for integrating K-type thin-film strain gauges, which are to be microfabricated at LundNanoLab, onto polished stainless steel substrates. Specifically:

- Gain hands-on experience with microfabrication principles and cleanroom tools at LundNanoLab.
- Perform REFLEX sugar-assisted transfer of K-type thin-film sensor structures (5 nm Ni adhesion layer, 140 nm Chromel, 140 nm Alumel) from silicon donor substrates onto polished stainless steel receiver substrates.
- Characterise the transferred structures using optical microscopy, scanning electron microscopy (SEM), and atomic force microscopy (AFM) to assess structural integrity.

1.3 Limitations

The scope of this project introduces several practical boundaries. Firstly, the study is limited to stainless steel substrates while transfers onto large scaled curved or industrial surfaces are not attempted. Electrical probing of the transferred sensors to gather resistance measurements and thermoelectric calibration data is outside the primary goals of this work. In addition, mechanical strain testing of the transferred structures is not performed. Finally, the work is constrained by the time frame of a 15-credit BSc project, and the results should be interpreted within this context.

2 Theory and Background

2.1 Principles of Transfer Printing

Transfer printing is simply described as a method in which micro- or nanostructures produced on a donor substrate under controlled cleanroom conditions, are relocated onto a receiver substrate of arbitrary geometry via an intermediate carrier medium [5]. For a transfer to succeed, the adhesion between the structure and the carrier (sugar in our case) must exceed the adhesion between the structure and the donor during separation. On the other hand, during deposition, it must be weaker than the adhesion between the structure and the receiver [6, 7].

The thermodynamic work of adhesion W_A between two surfaces in contact is given by:

$$W_A = \gamma_1 + \gamma_2 - \gamma_{12} \tag{1}$$

where γ_1 and γ_2 are the surface energies of the two materials and γ_{12} is the interfacial energy of the joined pair [7]. A successful transfer therefore requires that W_A at the carrier-film interface exceeds W_A at the film/donor interface during retrieval, and falls below W_A at the film/receiver interface during deposition.

The most widely established approach uses elastomeric polydimethylsiloxane (PDMS) stamps, where the effective adhesion is modulated by peel rate. Faster peeling increases adhesion for retrieval from the donor, while slow peeling reduces it for deposition onto the receiver [6].While effective on flat or minimally curved receiver surfaces, solid stamps cannot accommodate the area changes that arise on highly curved or extremely rough

surfaces. [4, 5]. Furthermore, the contact pressures required to retrieve fragile thin-film structures tend to damage the structures themselves. As an alternative, liquid-based carriers improve conformability but introduce uncontrolled surface displacements that compromise placement accuracy and intended positioning of the structures [4].

2.2 The REFLEX Process

The REFLEX (REflow-driven FLEXible transfer) process, introduced by Zabow [4], was developed to overcome the conformability limitations of solid-carrier methods by using a thermally reflowable sugar mixture as the carrier medium. The sugar combines the macroscopic rigidity of a solid carrier with the ability to conform around surfaces of arbitrary curvature by transitioning into a viscous fluid.

The sugar carrier is a combined 2:1:1 ratio by mass solution of table sugar (sucrose), corn syrup, and deionised water, heated to caramelisation at approximately 170–180 °C [4]. Corn syrup is added to inhibit crystallisation of the sucrose, which would otherwise produce an inhomogeneous, granular surface incompatible with the micrometre-scale precision required for transfers [4, 8]. Post caramelisation, the mixture is dissolved 1:1 with deionised water to produce a working sugar solution that can be stored for months.

The transfer process proceeds in five stages:

1. **Coating.** The diluted sugar solution is poured over a donor substrate, where the target microstructures lie on top of an acetone-soluble sacrificial layer.

2. **Drying.** The now coated donor substrate is placed in an oven at approximately 100 °C overnight to evaporate the water content and harden the sugar into a solid, glassy toffee. [4].

3. **Release.** The hardened sugar deposit is then immersed in acetone, which dissolves the sacrificial layer beneath the microstructures but not the sugar itself. The film is then peeled away from the donor, carrying the microstructures embedded in its underside.

4. **Reflow.** The sugar is then placed on the receiver substrate and gently heated to 35–50 °C. Here, the sugar softens into a highly viscous fluid and creeps conformally over the receiver surface, coating complex topographies including sharp edges, vertical sidewalls, and curved surfaces down to nanoscale radii of curvature [4, 8].

5. **Dissolution.** Once the microstructures have been deposited on the receiver, the sugar is dissolved with deionised water, leaving the transferred structures in place with no chemical residue at the interface [4].

The key advantage of sugar as a carrier is its solubility with water and resistance to acetone [4]. Utilizing the above method, Zabow demonstrated the transfer of arrays of 1 µm gold microdisks onto metals, glass, plastics, paper, semiconductors, elastomer, hydrogel, and biological surfaces including individual human hairs (75 μm diameter) and red blood cells (7–8 μm), with pattern alignment errors below 1° and pattern mismatches within one part per hundred even when the local surface area changed by over 300 % [4]. Additionally, [9] demonstrated sugar-mediated transfer of Au nanomeshes, Ag nanowire films, graphene, and MoS_2 onto both rigid and flexible substrates without organic solvents.

Temperatures involved play a key role, as if the baking step during drying is too aggressive, thermal stress in the sugar film can cause embedded microstructures to deform before solidification. And if the reflow temperature is too high, the sugar flows too rapidly, introducing displacements of the embedded structures. [4].

2.3 Donor Structures: K-Type Thin-Film Strain Gauges

The donor structures in focus of this project are referred to as K-type thin-film strain gauges microfabricated at LundNanoLab on silicon wafers. Each sensor consists of a stack of three deposited layers: a 5 nm nickel (Ni) adhesion layer, followed by either 140 nm of Chromel ($Ni_{90}Cr_{10}$) which forms the positive electrode, or 140 nm of Alumel ($Ni_{95}Al_2Mn_2Si_1$) which forms the negative electrode of the K-type thermocouple [1]. The Chromel and Alumel poles are patterned into a gauge geometry and meet at a junction where temperature can essentially be measured.

2.3.1 Role of the Nickel Adhesion Layer

A thin adhesive layer is standard practice in the deposition of metallic thin films onto oxide surfaces such as SiO_2 [7]. Without it, the conjunction of the alloy film and the substrate is weak, causing poor liftoff behaviour during the methodology. Nickel was chosen as the adhesion layer in this project because it is the dominant element in both Chromel (90 % Ni) and Alumel (95 % Ni), ensuring chemical compatibility of the adhesion layer/alloy interface and avoiding the introduction of a foreign element at the thermoelectric junction that could perturb the sensor's thermoelectric properties [1, 10]. At 5 nm, the layer is sufficiently thin to promote adhesion without contributing meaningfully to the total film stress or thermoelectric signal. Additionally, the Ni adhesion layer allows for cleaner liftoff as it serves to weaken the film's adhesion to the donor substrate.

2.3.2 Sample Variants: Old and New Deposition Routes

Over the course of the experiments two variants of the donor sensors were produced, differing in the following:

- **Sample variant A** The 5 nm Ni adhesion layer was deposited by thermal evaporation. The sample was then removed from the deposition chamber and transferred through air before the Chromel and Alumel layers were sputtered in a later session. During its exposure to air, the Ni surface underwent oxidation, forming a native nickel oxide (NiO) layer at the Ni/alloy interface.
- **Sample variant B** Here, all three layers of Ni (now 10 nm), Chromel, and Alumel were deposited within a single uninterrupted sputtering session. This preserves a clean, oxide-free metal-to-metal layering throughout the film stack.

2.3.3 Residual Stress in Sputtered Thin Films

Thin films which are deposited by sputtering are subject to residual stress arising from either *intrinsic stress*, which develops during film growth due to ion-bombardment compaction, and grain boundary formation, or *extrinsic (thermal) stress*, which arises when cooling from the deposition temperature causes a mismatch in thermal expansion coefficients

between the film and the substrate [7]. The total biaxial residual stress σ_r in the film determines the strain energy release rate G available to propagate an interfacial crack:

$$G = \frac{(1 - \nu_f)\,\sigma_r^2\,h_f}{E_f} \tag{2}$$

where E_f is the Young's modulus of the film, ν_f is its Poisson's ratio, and h_f is the film thickness [7]. If G falls below the adhesion energy of the film substrate interface, the stored residual stress is insufficient to cause the film to spontaneously peel from the donor substrate. However, the additional thermal stress introduced during the sugar reflow step, where the metallic film and sugar carrier expand at different rates upon heating, superimposes on the existing residual stress state. If the reflow temperature is too high, this combined stress can cause the thin-film legs to deform before the sugar has dissolved.

2.3.4 The Seebeck Effect and Thermoelectric Sensing

When two dissimilar metallic conductors are joined at one end (the hot junction) and their free ends are held at a different temperature (the cold junction), a thermoelectric electromotive force (EMF) is induced. This arises because charge carriers in each material diffuse away from the hotter region at a rate that depends on the material's electronic band structure, generating a net charge imbalance. The output EMF is related to the temperature difference $\Delta T = T_{\text{hot}} - T_{\text{cold}}$ by the differential Seebeck coefficient S_{AB}:

$$V = S_{AB}\,\Delta T, \qquad S_{AB} = S_A - S_B \tag{3}$$

where S_A and S_B are the absolute Seebeck coefficients of the two thermocouple poles [1, 11]. For bulk K-type wire thermocouples (Chromel/Alumel), $S_{AB} \approx 41\,\mu\text{V}/^\circ\text{C}$ in the range 0–400 °C [12].

In thin-film thermocouples, S_{AB} generally has a reduced value. Liu et al. [11] showed that for NiCr/NiSi thin-film thermocouples, the Seebeck coefficient increases from 7.32 to $13.36\,\mu\text{V}/^\circ\text{C}$ as film thickness increases from 400 to 2000 nm, remaining well below the bulk wire value of $\sim 40\,\mu\text{V}/^\circ\text{C}$ throughout. The dominant mechanism is that thinner films contain fewer free electrons through their thickness, reducing the number of charge carriers available to drive the thermoelectric effect [11] At the 140 nm film thickness used in this project, a significant reduction in S_{AB} relative to the bulk K-type value is therefore expected.

2.3.5 The Gauge Factor

When deformed, metallic conductors alter their electrical resistance. For a gauge element of length L, cross-sectional area A, and resistivity ρ, the resistance is given by $R = \rho L/A$. Under uniaxial strain ε, R changes due to both a geometric deformation, the conductor becomes longer and thinner, and a change in resistivity due to lattice deformation. The combined sensitivity is expressed by the gauge factor:

$$\text{GF} = \frac{\Delta R/R}{\varepsilon} = 1 + 2\nu + \frac{\Delta\rho/\rho}{\varepsilon} \tag{4}$$

where ν is Poisson's ratio of the gauge material [3, 13]. For metallic thin films the contribution through resistivity is small, hence the gauge factor is dominated by the geometric term and takes a value of approximately 2 [3, 13]. The NiCr-family alloys

including Chromel ($Ni_{90}Cr_{10}$) are well established as strain gauge materials because their gauge factor remains stable near 2 across a wide range of temperatures and film thicknesses [13].

2.3.6 Temperature Coefficient of Resistance

The resistance of a metallic conductor also changes with temperature through the temperature coefficient of resistance (TCR), defined as:

$$\mathrm{TCR} = \frac{1}{R_0}\frac{\Delta R}{\Delta T} \tag{5}$$

where R_0 is the resistance at a reference temperature [3]. In a strain measurement, a temperature change produces a resistance change that cannot be distinguished from a mechanical strain signal without additional information. In a K-type thin-film sensor the thermoelectric junction provides an independent temperature measurement from the same element. This allows the thermally induced resistance change to be estimated and subtracted from the total signal, which is the key advantage of the dual-function configuration.

2.4 Target Substrate: Stainless Steel

As forementioned, austenitic stainless steel (AISI 316 L) is selected as the receiver substrate in this study due to its widespread use in industrial applications and its relevance to thin-film sensor integration [1]. Upon air exposure, the surface spontaneously forms a native passive oxide layer approximately 1–3 nm thick [7]. This oxide layer determines the surface chemistry and energy of the substrate, which in turn influences the interfacial adhesion available to retain the transferred film in place.

3 Experimental Methods

The experimental procedures for both sample variants are below.

3.0.1 Donor Substrate Preparation

The K-type thin-film strain gauge samples were received as diced silicon chips post the fabrication process, each carrying patterned Chromel (K+) and Alumel (K−) gauge poles on a 5 nm Ni adhesion layer. Prior to sugar coating, each donor chip was cleaned with acetone and isopropanol (IPA) utilising a wet bench. Acetone removes organic contaminants and any photoresist residues remaining from the microfabrication process, while IPA is used as a rinsing agent to remove acetone residues without leaving water marks. The chip was subsequently dried with nitrogen (N_2) gas to prevent moisture contamination and ensure a clean surface prior to sugar coating. Post cleaning, the chip was inspected under the optical microscope to confirm that the Chromel and Alumel gauge features were intact and well-defined prior to proceeding.

Polished stainless steel substrates were used as the receiver in all transfer experiments and were cleaned using the same acetone and IPA wet bench procedure applied to the donor chips. Cleaning was performed right before transfer to minimise the presence of airborne contaminants onto the reactive oxide surface.

3.0.2 REFLEX

The sugar solution was prepared as described in Section 2.2 (prepared prior to the start of this project). The cleaned donor chip was placed on a flat surface and 1-3 drops of the sugar solution were applied to fully cover the gauge features. The volume was varied to produce a film of varying thickness.

The coated chip was transferred to an oven and baked at 110 °C for 12 hours to evaporate the water content and harden the sugar into a solid glassy film. For sample variant A, the oven used had no programmable ramp setting, reaching 110 °C in approximately 30 minutes from room temperature. For sample variant B, the temperature was ramped at a controlled rate of 5 °C min^{-1} before being held at 110 °C for 12 hours. In both cases, the chip was subsequently allowed to cool slowly inside the oven.

Following baking, the donor chip was removed from the oven and inspected under the optical microscope. This intermediate inspection step was used to assess the condition of the Chromel and Alumel gauge features beneath the sugar layer.

The liftoff of the hardened sugar film was performed using a combination of a scalpel and fine-tipped tweezers. The scalpel was used to carefully score and separate the edge of the sugar film from the donor chip surface, after which the tweezers were used to carefully peel the film away. The sugar fragments were scanned under an optical microscope to view the condition of the structures embedded.

The lifted sugar film, carrying the K-type gauge structures on its underside, was positioned manually onto an area of the cleaned stainless steel receiver substrate using tweezers, with the gauge features facing downward toward the steel surface. The substrate was then placed on a hotplate and heated gently to 70 °C to induce reflow of the sugar carrier until it softened and adhered, bringing the embedded microstructures into contact with the stainless steel.

Once the transferred structures had adhered to the stainless steel surface and the sample had cooled, the remaining sugar carrier was dissolved by immersing in water. This left the transferred structures on the receiver substrates.

3.1 Characterisation Techniques

3.1.1 Optical Microscopy

Optical microscopy was used throughout the project as the primary tool for rapid and simple inspection of both donor and receiver surfaces before and after each process step. It provided an overview of the embedded pattern geometry and the spatial extent of transfer outcomes across the receiver substrate, enabling identification of regions for higher resolution follow-up characterisation.

3.1.2 Scanning Electron Microscopy (SEM) and Energy Dispersive X-ray Spectroscopy (EDS)

Scanning electron microscopy was used to image surface morphology at resolutions beyond the optical diffraction limit, providing detailed information on the Chromel and Alumel poles, the presence of cracking, and the conformality between the structures and the stainless steel surface. Imaging was performed using two complementary detector modes: the UD detector, a secondary electron detector positioned within the column, providing surface-sensitive imaging with high spatial resolution for resolving fine topographical features; and the MD detector, operating in backscattered electron mode and yielding

elemental contrast whereby regions of higher atomic number appear brighter relative to lighter elements. EDS was used in conjunction with SEM to map the elemental composition of transferred structures and remnants on the donor substrates. Access to both instruments at LundNanoLab required completion of formal operator training and obtaining a licence prior to use.

3.1.3 Wet Bench Processing

Wet bench facilities at LundNanoLab were used for solvent cleaning of both donor and receiver substrates. Access required completion of chemical safety training and a wet bench operating licence prior to use. The cleaning procedure itself is described in Section 3.0.1.

4 Results & Discussion

The results presented in this section are based on optical microscopy, SEM, EDS images acquired at LundNanoLab throughout the transfer printing process where the two sample variants were investigated. Images range from sugar layers still adhered to the donor substrates post baking, sugar layers lifted off donor substrates, and transferred structures on stainless steel.

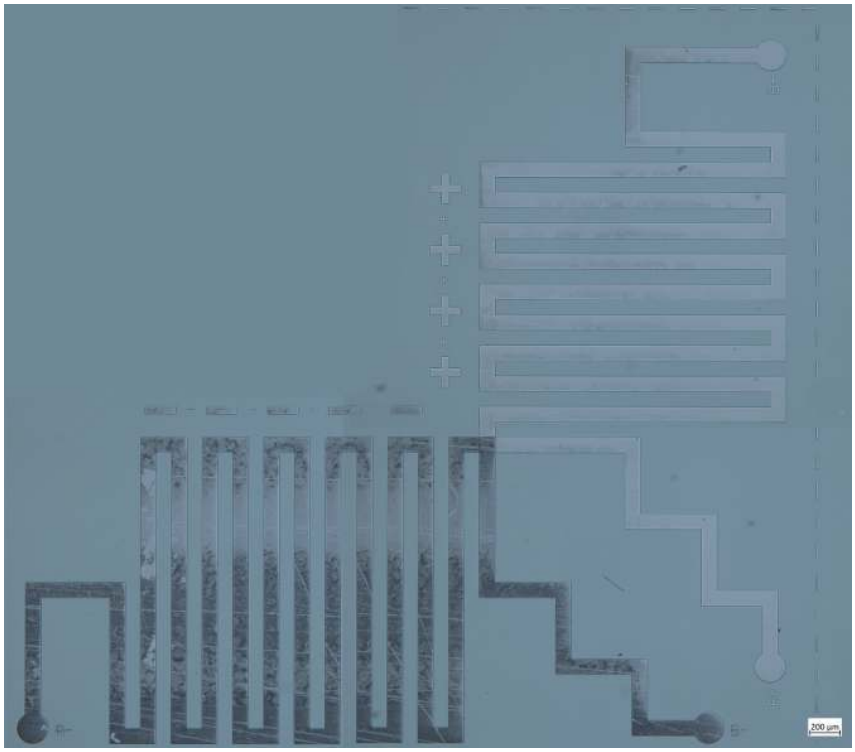

Figure 1: Optical micrograph of the full K-type thin-film strain gauge donor chip prior to sugar coating, showing the complete gauge geometry including the Chromel (K+) serpentine pole array (top right), the Alumel (K−) pole array (bottom), and the thermocouple junction region (centre). The image is a composite of four overlapping micrographs. Scale bar: 200 µm.

4.1 Optical Microscopy

Two donor chips from sample variant A were subjected to the sugar coating and baking procedure described in Section 3.0.2. One chip received a thin sugar layer of 1-2 drops, while the other received a thick layer of 3-4 drops. This was done to assess how sugar film thickness affects the mechanical integrity of the film during liftoff. Additionally, the oven was set to target temperature of 110 °C requiring 40 minutes to reach from room temperature. Figures 2 and 3 show optical micrographs of regions from the thin and thick layer chips respectively, captured immediately after the liftoff attempt.

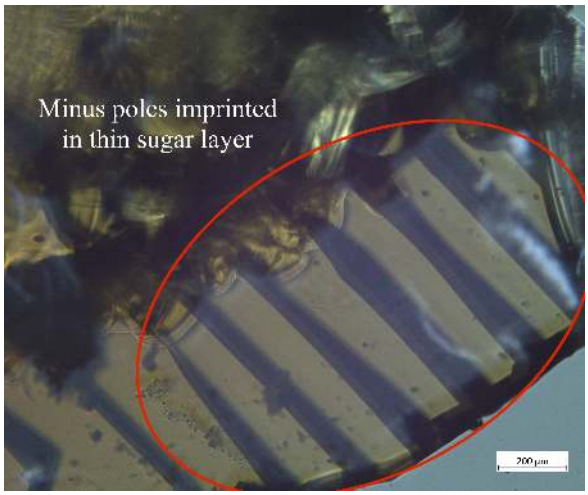

(a) Alumel (K-) pole region

(b) Chromel (K+) pole region

Figure 2: Optical micrographs of the thin sugar layer on the sample variant A donor chip following attempted liftoff. (a) shows the array of Alumel (K−) microstructures which were successfully retrieved and remained embedded in the sugar film, retaining the pattern geometry from the donor without displacement during hardening. (b) shows the lifted sugar film, where only fragments of the Chromel (K+) poles were retrieved, alongside identation of the structural mould left in the sugar surface. Scale bars: 200 µm.

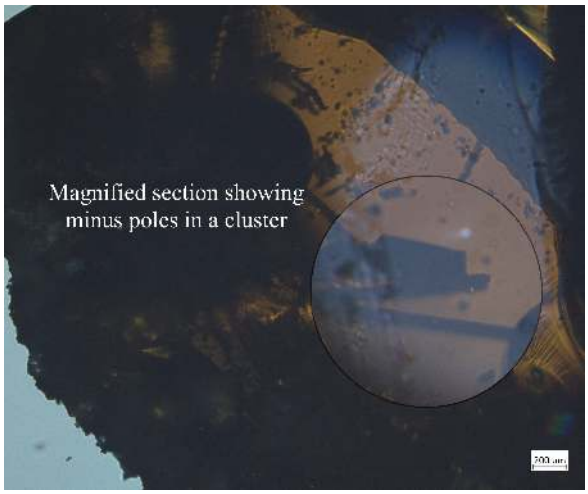

(a) Region 1.

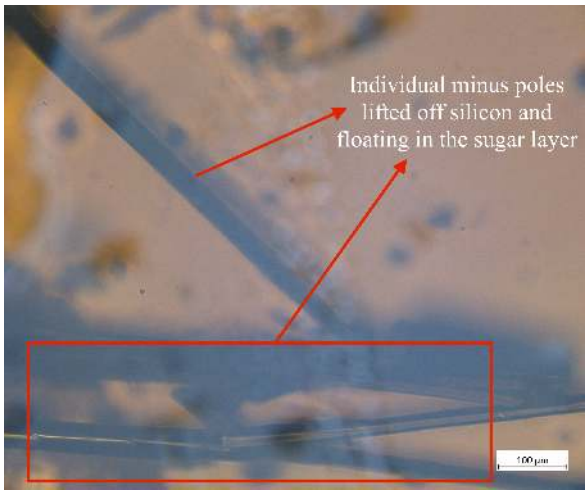

(b) Region 2.

Figure 3: Optical micrographs of the thick sugar layer from the sample variant A donor chip following attempted liftoff.(a) shows a wide-field view of a lifted sugar film fragment, with a magnified region revealing a cluster of Alumel (K−) poles that were successfully retrieved from the donor. (b) shows a higher magnification view of individual K− poles that lifted off the silicon donor and displaced within the sugar during hardening, losing their original array geometry. Scale bars: ((a) 200 µm, (b) 100 µm.

In both cases, the sugar film fractured during peeling rather than releasing as a continuous freestanding layer. The Alumel (K−) poles were retrievable by the sugar carrier in both the thin and thick layer cases, while the Chromel (K+) poles remained adhered to the donor substrate and could not be lifted as evident in figure 2 (b) where only fragments were embedded. In the thin layer case the K− poles retained their original array geometry, whereas in the thick layer case they displaced and clustered during the drying stage. This displacement observed in figure 3 (a) & (b) indicates that the thicker sugar layer, while providing greater mechanical robustness during peeling, introduced sufficient fluid motion during the baking and drying stages to disturb the positions of the retrieved structures before solidification.

The selective retrieval of Alumel but not Chromel poles can be attributed to the difference in interlayer adhesion between the two alloys and the underlying Ni adhesion layer. During the air exposure period between the evaporation and sputtering steps in the old sample fabrication route, the 5 nm Ni adhesion layer oxidised in the environment to form a native NiO surface layer [14]. When Chromel was sputtered onto this surface, the 10 % Chromium content of the alloy, which is highly reactive toward oxygen, is readily forming Cr_2O_3 at oxide interfaces [15]. This resulted in strong oxide-on-oxide bonding at the Chromel/NiO intersection. This increased the adhesion energy beyond what the sugar carrier could overcome during hardening and peeling. Furthermore, although Alumel does contain a small amount of aluminium, the significantly lower Al content means that any Al_2O_3 formation would be minimal compared to the Cr_2O_3 on Chromel, further reducing interfacial bond strength. Together, these factors present a weaker film-sugar interface that the sugar carrier successfully ruptured during peeling, consistent with the selective retrieval of K− poles observed across both layer thicknesses in the old sample variant, while K+ poles remained adhered to the donor in all cases. This is consistent with the selective retrieval of K− poles observed across both layer thicknesses in the old sample variant, while K+ poles remained adhered to the donor in all cases.

The following images show results from the sample variant B, (Section 3.0.1). Similar to the previous attempt, two donor chips from the new variant were coated with sugar, one receiving a thin layer and the other a thick layer. However, The baking step was performed in a programmable oven with controllable temperature ramp rate. The oven was ramped from room temperature to 110 °C at a rate of 5 °C min^{-1} and held at 110 °C for 12 hours, after which the sample was cooled slowly inside the oven. Figures 4 and 5 show optical micrographs of the Chromel and Alumel gauge features on the thick and thin layer chips respectively, imaged through the baked sugar layer prior to liftoff.

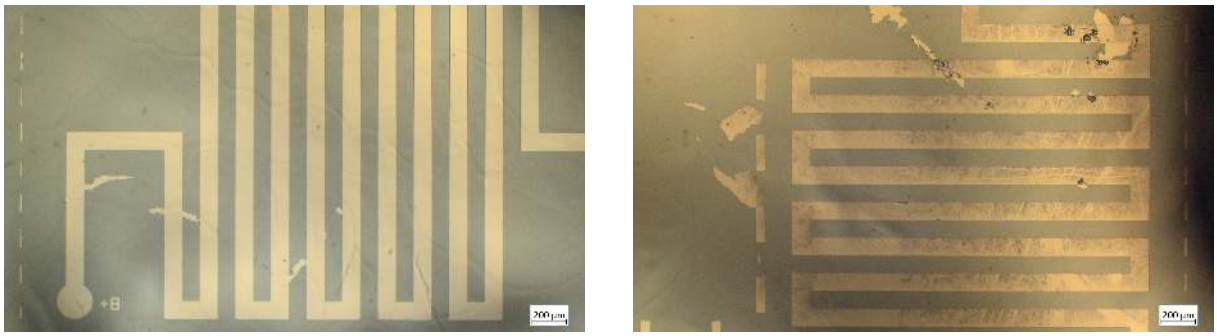

(a) Chromel (K+) pole. (b) Alumel (K−) pole.

Figure 4: Optical micrographs of sample variant B's donor chip following baking at $\sim$ 110 °C for 12 hours, with the thin sugar layer still in place on the substrate. (a) shows the Chromel (K+) pole region and (b) shows the Alumel (K−) pole region. Scale bars: 200 µm.

This result differs from the sample variant A, where a thin sugar layer was sufficient to embed and retrieve the Alumel poles, indicating that the absence of the vacuum break in sample variant B may have altered the interfacial adhesion conditions at the film/sugar interface. In contrast to this, the thick sugar layer on this new sample variant donor chip showed clear evidence of interaction with both gauge legs during baking, as shown in Figure 5.

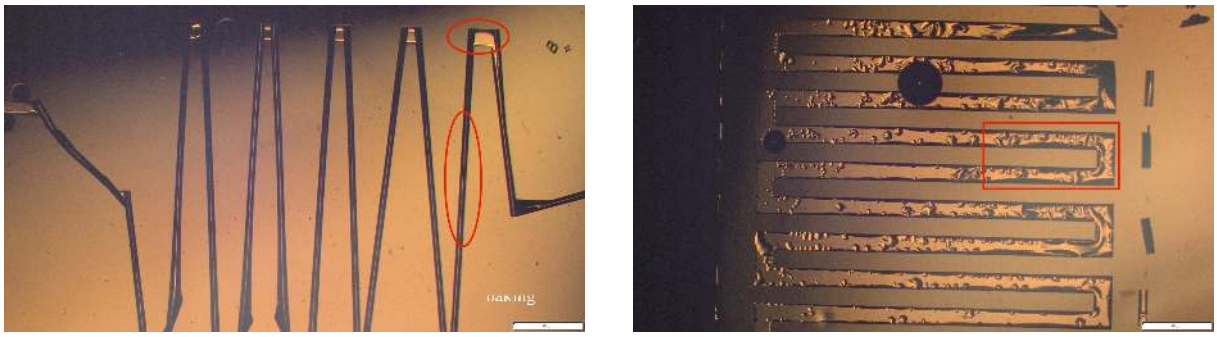

(a) Chromel (K+) pole. (b) Alumel (K−) pole.

Figure 5: Optical micrographs of the sample variant B donor chip following baking at 110 °C for 12 hours, with the thick sugar layer still in place on the substrate. Images were taken prior to liftoff from the silicon donor. (a) shows the Chromel (K+) pole region, where the poles display pronounced out-of-plane warping along the z-axis, appearing narrower in the top-down view due to vertical deformation while retaining their in-plane pattern geometry. (b) shows the Alumel (K−) pole region, where the poles exhibit crater-like surface indentations within the sugar but largely retain their original lateral geometry. Scale bars: 10 µm.

Since the thin sugar layer on sample variant B proved insufficient to retrieve both poles, the subsequent batch of donor chips was prepared with a thin layer consisting of an increased number of sugar solution drops, while the thick layer volume was kept identical to that used in the preceding batch. This adjustment aimed to increase the sugar layer thickness in the thin variant, improving mechanical contact and adhesion at the film/sugar interface without altering the conditions of the thick layer experiment.

(a) Chromel (K+) pole. (b) Alumel (K−) pole.

Figure 6: Optical micrographs of the subsequent sample variant B donor chip following baking at ∼ 110 °C for 12 hours, with the thin sugar layer still in place on the substrate. (a) shows the Chromel (K+) pole region and (b) shows the Alumel (K−) pole region. Scale bars: 200 µm.

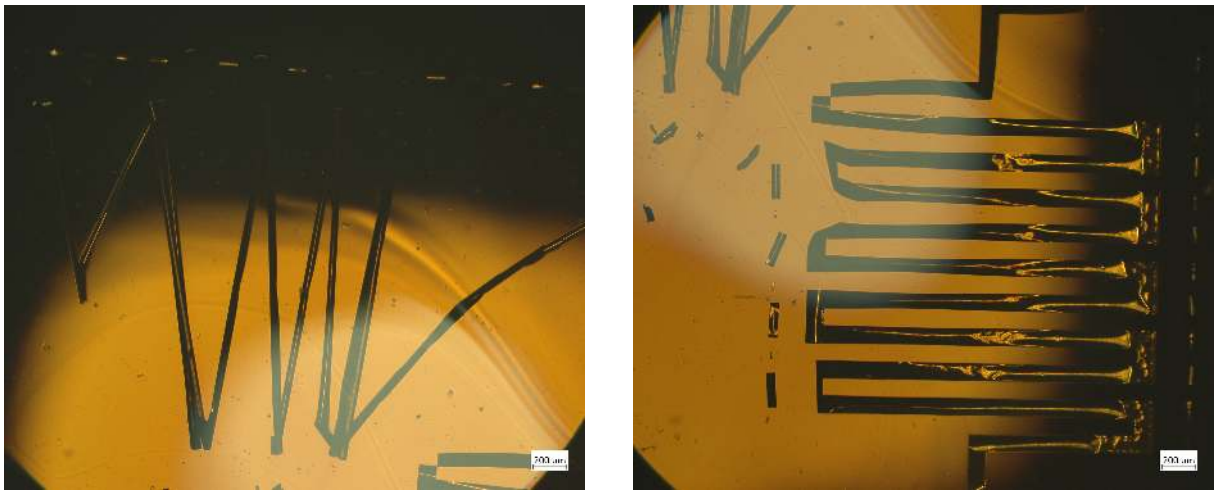

(a) Chromel (K+) pole. (b) Alumel (K−) pole.

Figure 7: Optical micrographs of the subsequent sample donor chip following baking at 110 °C for 12 hours, with the thick sugar layer still in place on the substrate. Images were taken prior to liftoff from the silicon donor. (a) shows the Chromel (K+) pole region and (b) shows the Alumel (K−) pole region. Scale bars: 200 µm.

The thick sugar layer results from the new sample variant reveal warping, which is likely attributed to thermally induced stress during the baking step, consistent with the thermal expansion mismatch between the metallic film and the sugar carrier. Both poles show physical deformation, the Chromel poles warped out of plane and floating inside the hardening sugar layer, while the Alumel poles housed indentations and minimal warping before liftoff was even attempted. This is attributed to the thermal expansion mismatch between the metallic film and the sugar carrier at the baking temperature, as discussed in the section on residual stress. Notably, reducing the ramp rate to 2 °C min^{-1} was observed to produce comparable or greater deformation, suggesting the warping is governed by the peak temperature reached rather than the rate at which it is approached. The absence of a vacuum break in the new samples means the Ni/alloy boundaries are clean and oxide-free. This may have reduced the adhesion of the film stack to the donor substrate sufficiently that thermally induced stress during baking caused the films to buckle rather than remain pinned. As observed, the thin layer in this new sample variant showed no such deformation, consistent with insufficient sugar volume to grip and stress the films at this thickness. Taken together, the new sample results suggest that while eliminating the vacuum break addresses the adhesion asymmetry seen in the old samples, the baking temperature and gradient requires optimisation to prevent thermally induced deformation prior to liftoff.

4.2 Transfer Quality: Visual Inspection and Optical Microscopy

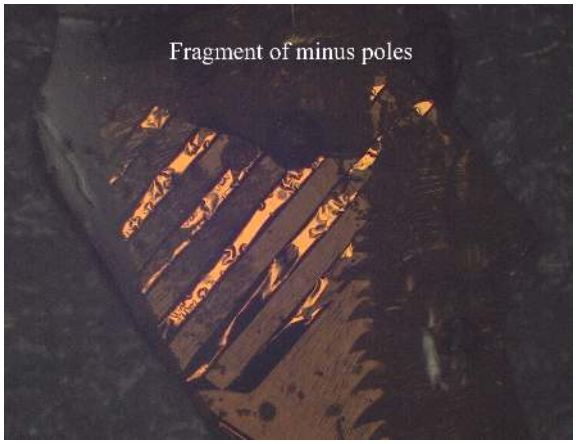

(a) Lifted sugar fragment containing Alumel (K−) poles.

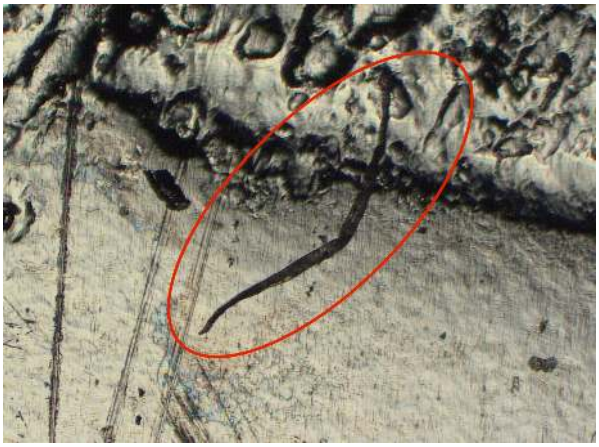

(b) Transferred Alumel (K−) pole on stainless steel substrate.

Figure 8: Optical micrographs showing the transfer of an Alumel (K−) pole from sample variant B's thick sugar layer onto a stainless steel receiver substrate. (a) shows the lifted sugar film fragment carrying embedded K− poles retrieved from sample variant B's donor chip. (b) shows a single Alumel pole successfully deposited on the polished stainless steel surface following reflow at $\sim 70\,^{\circ}\mathrm{C}$ and dissolution of the sugar carrier in water.

While Figure 8(b) confirms that transfer onto the stainless steel substrate is achievable in principle, with a single Alumel (K−) pole successfully deposited following reflow and sugar dissolution, the overall yield of this attempt was poor. Only one pole was recovered on the receiver substrate, indicating that the majority of the lifted sugar fragment did not release its embedded poles onto the steel surface as intended. This limited success is likely attributable to the small fragment size retrieved during liftoff, reducing the number of poles available for transfer, as well as potential insufficient contact between the sugar fragment and the receiver substrate during the reflow step. Nevertheless, the result demonstrates proof-of-concept for the transfer mechanism, motivating the subsequent batch with improved sugar layer preparation.

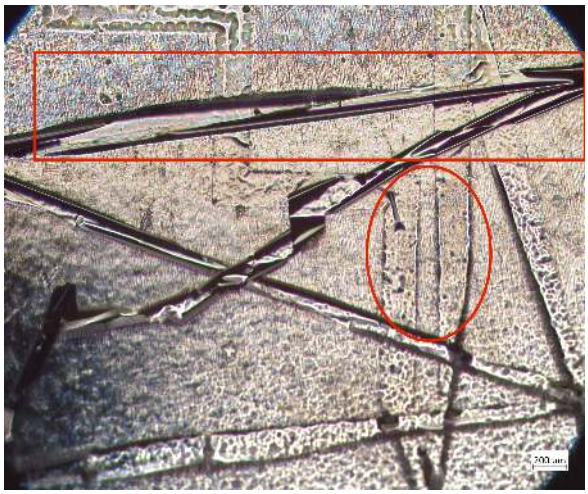

(a) Transferred poles from the thick sugar layer. The boxed region contains Chromel (K+) poles, while the circled region shows Alumel (K−) poles that retained their original lateral geometry following transfer.

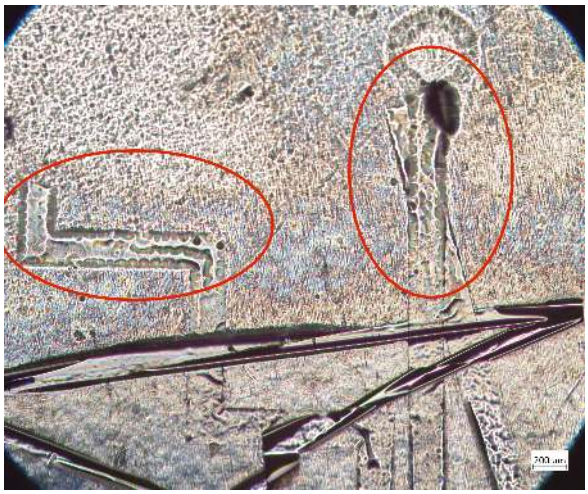

(b) Transferred Alumel (K−) poles from the thick sugar layer. The circled regions highlight individual minus pole sections that have been successfully deposited onto the stainless steel receiver substrate.

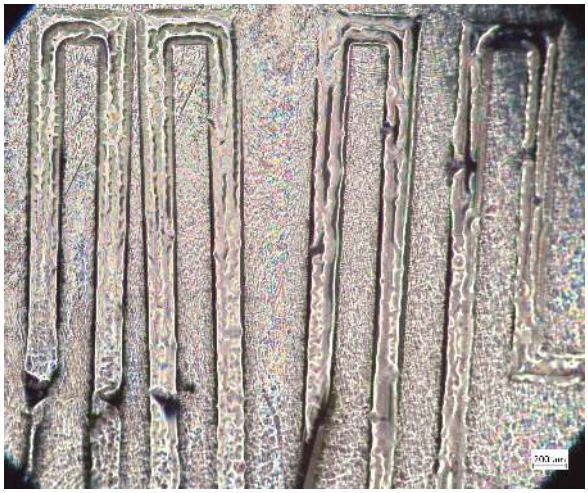

(c) Magnified view of the Alumel (K−) pole array from the thick sugar layer, corresponding to the geometry observed prior to liftoff in Figure 7. The poles retain their original serpentine pattern following transfer.

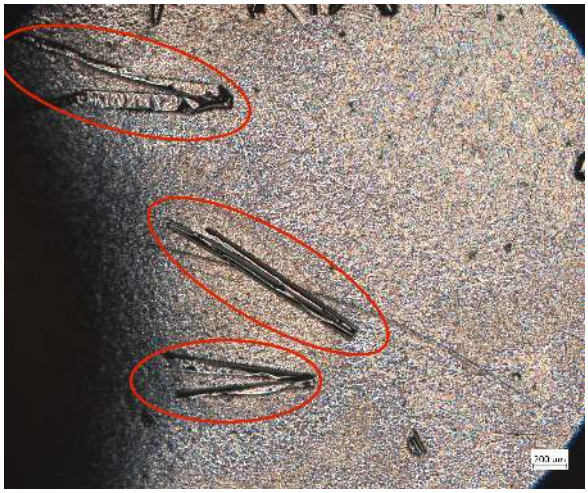

(d) Warped Chromel (K+) poles on the receiver substrate, highlighted by the circled regions. The poles display displacement during the reflow and sugar dissolution steps of the transfer process.

Figure 9: Optical micrographs showing the transfer of K-type thermocouple poles from the latest batch thick sugar layer onto a stainless steel receiver substrate. Scale bars: 200 µm.

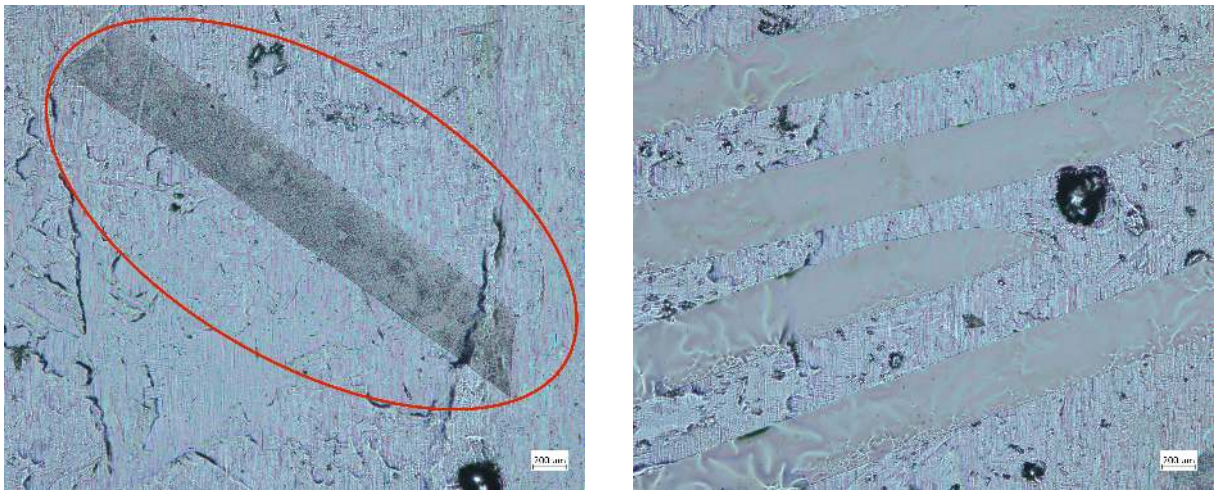

(a) (b)

Figure 10: Optical micrographs of Alumel (K−) poles from the latest batch thin sugar layer, corresponding to the geometry observed prior to liftoff in Figure 6(b), following transfer onto a polished stainless steel receiver substrate via reflow at $\sim 70\,^{\circ}\mathrm{C}$ and dissolution of the sugar carrier in water. Scale bars: 200 µm.

The transfer results demonstrate that the process was largely successful for the Alumel (K−) poles, which retained their original lateral geometry following reflow and sugar dissolution, as seen in Figures 9 and 10. This is consistent with the pre-liftoff micrographs in Figure 7(b), where the Alumel poles remained embedded at the base of the sugar layer with minimal out-of-plane deformation. Their position at the sugar-substrate interface ensured direct contact with the stainless steel receiver surface during the reflow step, facilitating adhesion. The Chromel (K+) poles, however, having warped out-of-plane and become suspended within the sugar layer during baking, were no longer in contact with the receiver substrate during reflow, preventing effective bonding. Consequently, during the water dissolution step, the detached Chromel poles were free to float and migrate within the dissolving sugar carrier, resulting in the scattered and distorted deposits observed in Figures 9(a) and 8(d). These results suggest that resolving the thermally induced warping of the Chromel poles prior to liftoff is a challenge for achieving a complete and geometrically faithful transfer of the full K-type thermocouple structure.

4.3 SEM Analysis

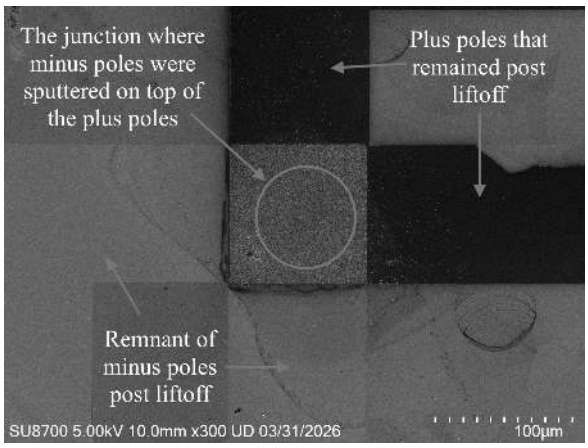

(a) Junction region, UD mode. Scale bar: 100 µm.

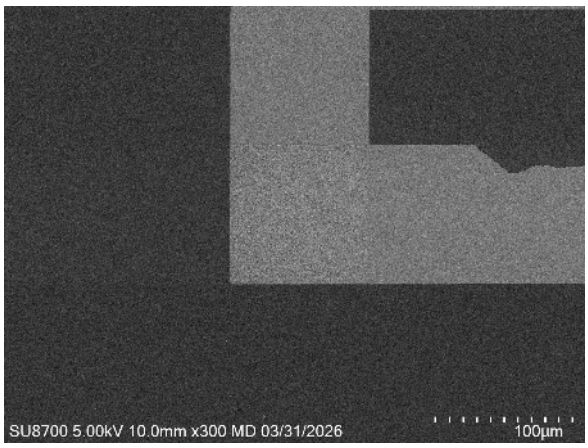

(b) Junction region, MD mode. Scale bar: 100 µm.

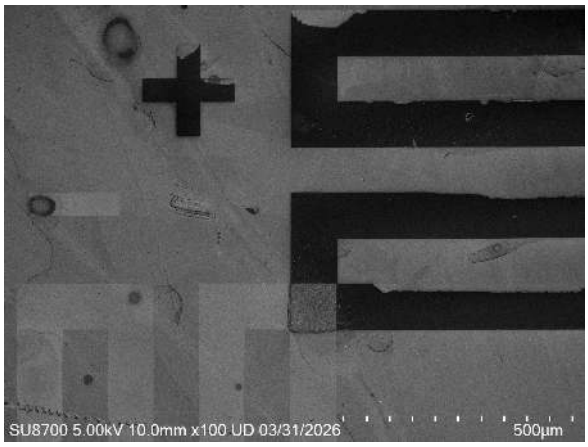

(c) zoomed out view, UD mode. Scale bar: 500 µm.

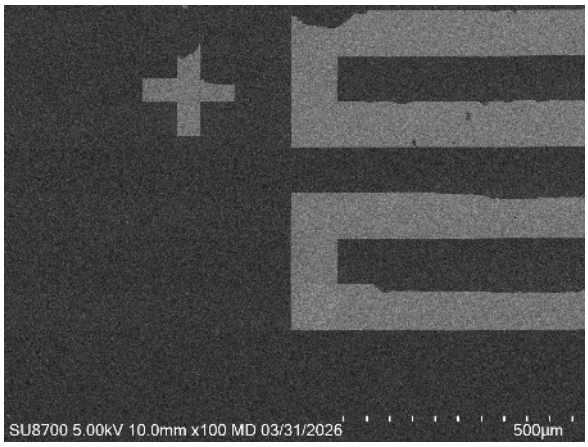

(d) zoomed out view, MD mode. Scale bar: 500 µm.

Figure 11: SEM images of the junction region where the Chromel (K+) and Alumel (K−) poles overlap on the sample variant A's thin sugar layer donor chip following attempted liftoff. (a) and (b) show the junction at higher magnification under each mode. (c) and (d) show a wider field of view of the same region under the corresponding modes.

The figure above shows SEM images of the junction region on sample variant A's thin sugar layer donor chip following liftoff. In the UD mode images (a) and (c), the Chromel (K+) poles appear dark, confirming that they remained adhered to the silicon donor substrate post-liftoff, consistent with the optical microscopy observations. The Alumel (K−) pole region shows only the remnant outline where the K- poles were successfully retrieved by the sugar carrier. In the MD mode images (b) and (d), the elemental contrast reveals the distinct material regions more clearly: the Chromel poles are visible due to their higher chromium content producing stronger backscatter signal, while the Alumel pole region is absent, confirming its removal during liftoff. The junction region, where the Alumel poles were sputtered on top of the Chromel poles during fabrication, is visible in both modes as a region of overlapping contrast.

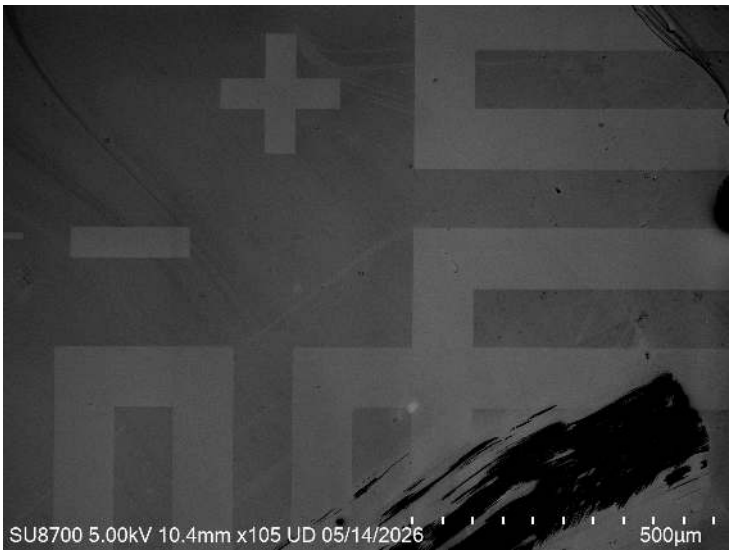

Figure 12: SEM image of the junction region where the Chromel (K+) and Alumel (K−) poles overlap on the latest batch sample variant B donor chip following attempted liftoff, imaged using the UD detector. Scale bar: 500 µm.

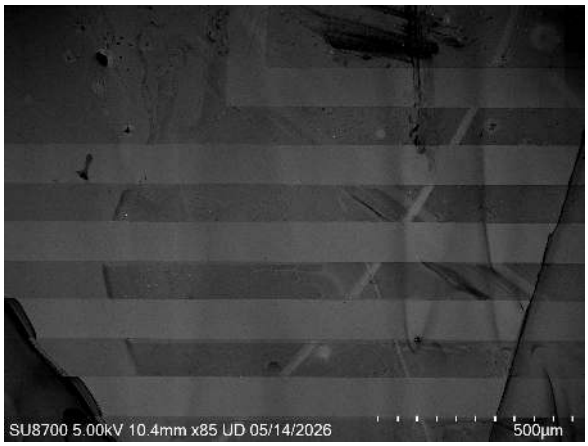

(a) Chromel (K+) pole region, UD mode. Scale bar: 500 µm.

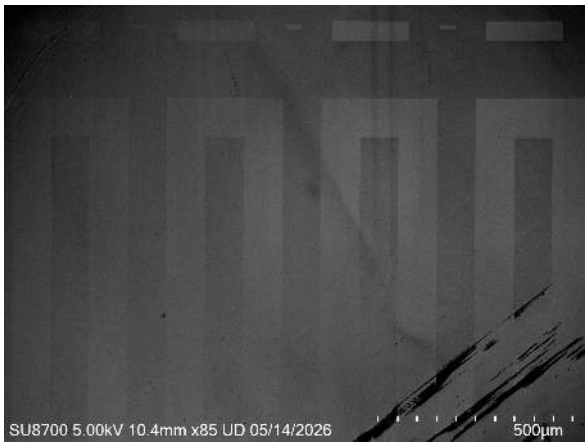

(b) Alumel (K−) pole region, UD mode. Scale bar: 500 µm.

Figure 13: SEM images of the Alumel (K−) and Chromel (K+) pole regions on the latest batch sample variant B donor chip following attempted liftoff, imaged using the UD detector.

Figures 12 and 13 show SEM images of the junction and pole regions on the latest batch sample variant B donor chip following liftoff. In contrast to sample variant A, where the Chromel (K+) poles remained visibly adhered to the donor substrate in the UD mode images, both the Chromel and Alumel pole regions in variant B appear largely absent from the donor surface following liftoff.

4.4 EDS Analysis

EDS mapping was performed on the same junction region as the SEM analysis, where the Chromel (K+) and Alumel (K−) poles overlap. At this junction the film stack from

bottom to top is: Ni adhesion layer, Chromel, Ni adhesion layer, Alumel. Following liftoff of the Alumel pole in the thin sugar layer old sample, EDS was used to determine whether the upper Ni adhesion layer was retrieved together with the Alumel or remained on the Chromel surface.

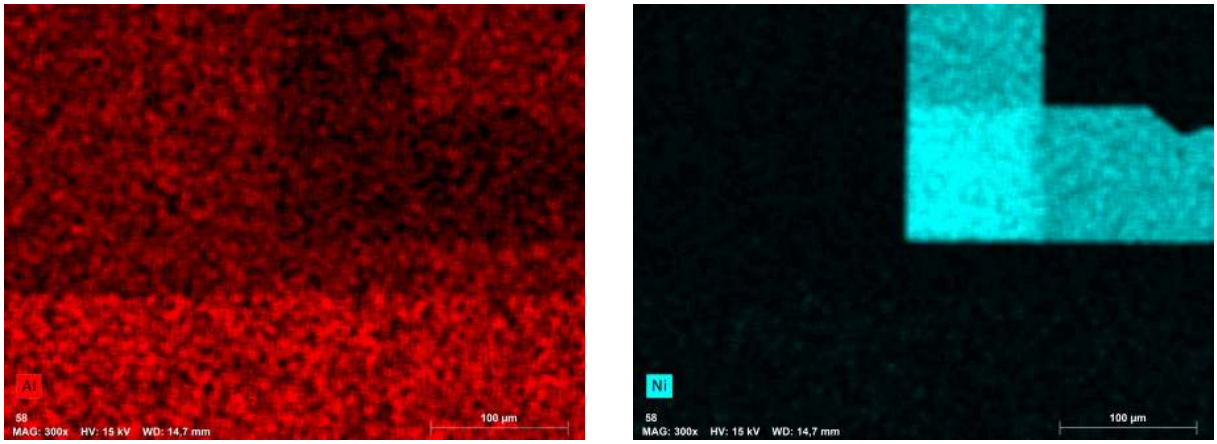

(a) Aluminium (Al) signal map. (b) Nickel (Ni) signal map.

Figure 14: EDS elemental maps of the junction region between the Chromel (K+) and Alumel (K−) poles on the old sample donor chip following liftoff. (a) shows the aluminium signal, (b) shows the nickel signal, Scale bars: 100 µm.

Figure 14 shows EDS elemental maps of the junction region following liftoff of sample variant A. The aluminium signal map in figure 14(a) shows a uniform distribution of dark regions across the mapped area, indicating that the Alumel (K−) material was successfully retrieved by the sugar carrier and is no longer present on the donor substrate. In contrast, the nickel signal map in figure 14(b) shows an elevated intensity at the junction region, suggesting that the 5 nm Ni adhesion layer beneath the Alumel poles was not retrieved during liftoff and remained on the donor substrate. This indicates that delamination occurred at the Alumel/Ni interface rather than at the Ni/silicon interface, meaning the sugar carrier ruptured the bond between the Alumel film and its adhesion layer, leaving the Ni behind. This is consistent with the relatively weak adhesion expected at a clean, oxide-free Ni/alloy boundary in the absence of a vacuum break, as discussed in Section 4.1.

The following EDS analysis was performed on the junction region of the latest batch sample variant B donor chip following liftoff, corresponding to the same area imaged by SEM in figure 12. Similar to sample variant A, elemental mapping was carried out to assess the abundance of Alumel and Ni adhesion layer remaining on the donor substrate post-transfer.

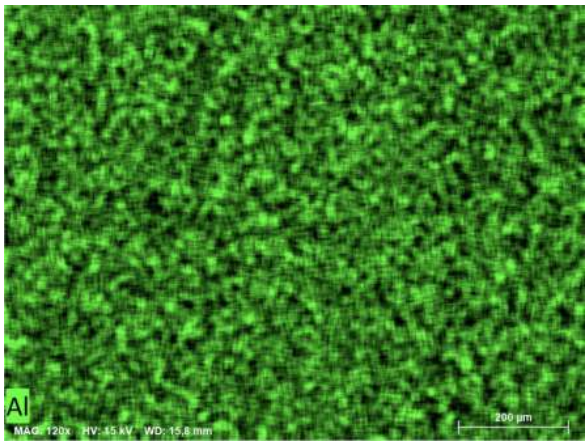

(a) Aluminium (Al) signal map.

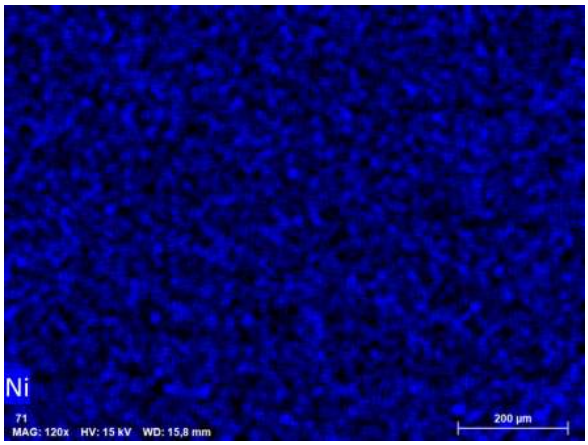

(b) Nickel (Ni) signal map.

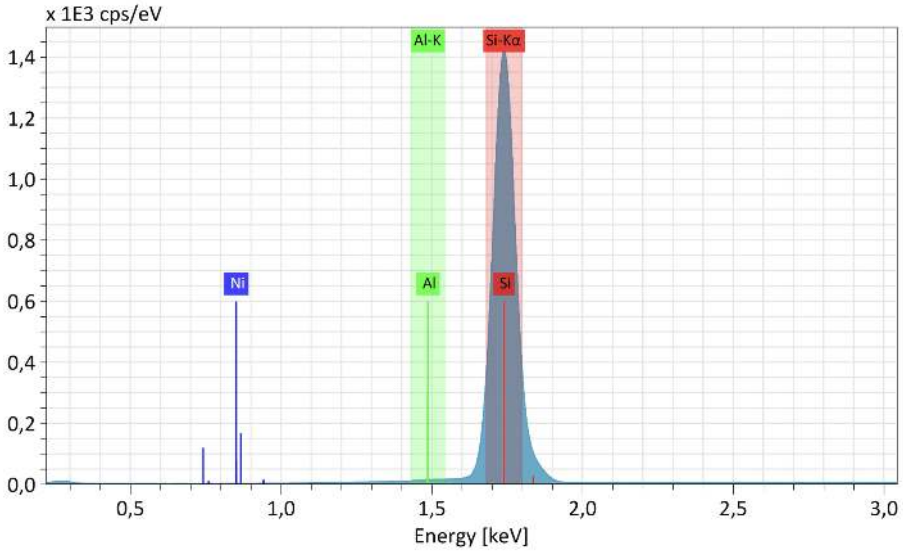

(c) EDS spectrum showing elemental peaks detected across the mapped region.

Figure 15: EDS analysis of the junction region on the latest batch sample variant B donor chip following liftoff. (a) shows the Al signal map, (b) shows the Ni signal map, both at a scale bar of 200 µm, and (c) shows the corresponding EDS spectrum.

Figure 15 presents the EDS elemental maps and spectrum of the junction region on the latest batch sample variant B donor chip following liftoff. The Al signal map in Figure 15(a) shows no localised aluminium signal across the mapped region, and similarly the Ni signal map in Figure 15(b) shows no elevated nickel concentration remaining on the donor surface. This is corroborated by the EDS spectrum in Figure 15(c), which is dominated by the Si-Kα peak originating from the silicon donor substrate, with only negligible Al and Ni signals detected. This indicates that both the Alumel (K−) film and the underlying 5 nm Ni adhesion layer were successfully retrieved during liftoff, leaving only the bare silicon substrate exposed. This is in contrast to sample variant A, where an elevated Ni signal was observed at the junction region post-liftoff, suggesting that delamination had occurred at the Alumel/Ni interface rather than the Ni/silicon interface. The complete removal of both layers in sample variant B suggests that the absence of a vacuum break resulted in a cleaner Ni/silicon interface with reduced adhesion, facilitating full retrieval of the film stack by the sugar carrier.

5 Outlook

This project and its results have demonstrated that sugar-assisted REFLEX transfer printing is a viable route for integrating K-type thin-film strain gauge structures onto polished stainless steel substrates, with successful deposition of geometrically intact Alumel (K−) poles confirmed by optical microscopy. Throughout the first few results, the adhesion asymmetry observed in sample variant A, where only the Alumel poles were retrievable, was attributed to strong oxide-mediated bonding at the Chromel/NiO interface arising from air exposure between deposition steps. Eliminating this vacuum break in sample variant B resolved the asymmetry, enabling retrieval of both poles. However, this introduced thermally induced warping of the Chromel poles during baking, governed by the peak baking temperature, which prevented their effective bonding to the receiver substrate during reflow. EDS analysis corroborated these findings, confirming full retrieval of both the Alumel film and the Ni adhesion layer in variant B, in contrast to the partial retrieval observed in variant A.

The primary outstanding challenge is resolving the thermally induced warping of the Chromel (K+) poles prior to liftoff. Future work should investigate lower baking temperatures or modified sugar formulations with a reduced glass transition temperature, to achieve sufficient hardening of the carrier without inducing deformation of the embedded film structures. Once warping is suppressed, complete transfer of a full K-type strain gauge, consisting of both Chromel and Alumel poles joined at a sensing junction, onto stainless steel should be achievable. Furthermore, this would enable electrical characterisation including resistance measurements and thermoelectric calibration of the Seebeck coefficient.

Beyond flat stainless steel substrates, the REFLEX method is well suited for extension to geometrically complex industrial surfaces such as cutting tool flanks, pipeline sections, and heat exchanger tubes, which build on the original motivation for this work. Transfer onto such surfaces would require optimisation of the reflow step to ensure conformal contact across the curvature, and surface preparation protocols tailored to each target material. Longer term, integration of such transferred sensors into a functional measurement system, with electrical contacts, signal conditioning, and in-situ strain or temperature readout, would realise the full scope of the approach demonstrated here.

Acknowledgements

I would like to thank my supervisor Anders Mikkelsen for introducing me to this project and for the scientific guidance and feedback that kept the work on track throughout the semester.

A huge thank you to my co-supervisor Ajsa Cuprija, who was there at every step of the experimental work. Ajsa demonstrated the full transfer printing procedure in the LundNanoLab cleanroom, helped with SEM and EDS when I had not yet obtained my operator licences, and was always available whenever doubts or questions came up. Her support and patience made a real difference to this project.

I would also like to thank Maksymilian Zaluski, who worked alongside me throughout the project. Maks showed great problem solving ability and gave important insights from his own experiments which helped attain the best results in our combined trials, and our collaboration made the whole process a lot smoother and more enjoyable.

Finally, I would like to thank the staff at LundNanoLab for providing access to the cleanroom facilities and equipment that this work depended on.

References

[1] A. Dalelkhan, F. Lenrick, A. Knutsson, and V. Bushlya. Advancing industry 4.0 with microfabrication of K-type TFTCs on stainless steel 316 L substrates: a study on SiO_2 insulation, substrate thickness, and surface roughness optimisation. *The International Journal of Advanced Manufacturing Technology*, 142:4745–4757, 2026. doi: 10.1007/s00170-025-17306-9.

[2] J.-F. Lei and H. A. Will. Thin-film thermocouples and strain-gauge technologies for engine applications. *Sensors and Actuators A: Physical*, 65(2–3):187–193, 1998. doi: 10.1016/S0924-4247(97)01683-X.

[3] H. Grange, C. Maeder, C. Bieth, S. Renard, and G. Delapierre. Thin film strain gauges on polymers: main characteristics. *Sensors and Actuators A: Physical*, 46–47: 213–217, 1995. doi: 10.1016/0924-4247(94)00888-S.

[4] G. Zabow. Reflow transfer for conformal three-dimensional microprinting. *Science*, 378(6622):894–898, 2022. doi: 10.1126/science.add7023.

[5] A. Carlson, A. M. Bowen, Y. Huang, R. G. Nuzzo, and J. A. Rogers. Transfer printing techniques for materials assembly and micro/nanodevice fabrication. *Advanced Materials*, 24(39):5284–5318, 2012. doi: 10.1002/adma.201201386.

[6] M. A. Meitl, Z.-T. Zhu, V. Kumar, K. J. Lee, X. Feng, Y. Y. Huang, I. Adesida, R. G. Nuzzo, and J. A. Rogers. Transfer printing by kinetic control of adhesion to an elastomeric stamp. *Nature Materials*, 5(1):33–38, 2006. doi: 10.1038/nmat1532.

[7] A. A. Volinsky, N. R. Moody, and W. W. Gerberich. Interfacial toughness measurements for thin films on substrates. *Acta Materialia*, 50(3):441–466, 2002. doi: 10.1016/S1359-6454(01)00354-8.

[8] G. Zabow. Microprinting on curved surfaces with sugar. *Matter*, 6(3):764–775, 2023. doi: 10.1016/j.matt.2023.01.012.

[9] T. Hong, T. Shi, Z. Tang, and G. Liao. Sugar transfer of nanomaterials and flexible electrodes. *International Journal of Smart and Nano Materials*, 11(1):61–74, 2020. doi: 10.1080/19475411.2020.1731622.

[10] A. Datta, X. Cheng, M. A. Miller, and X. Li. High temperature annealing effects on chromel (Ni90Cr10) thin films and interdiffusion study for sensing applications. *Thin Solid Films*, 516(12):4307–4311, 2008. doi: 10.1016/j.tsf.2007.12.150.

[11] Z. Liu, Q. Wang, S. Guo, H. Wang, W. Jiang, S. Liu, C. Liu, N. Wang, Y. Cui, and W. Ding. The preliminary exploration on change mechanism of Seebeck coefficient for NiCr/NiSi thin film thermocouple with different thickness. *Journal of Alloys and Compounds*, 931:167573, 2023. doi: 10.1016/j.jallcom.2022.167573.

[12] K. N. Satish, G. K. Ananthasuresh, G. Jagadeesh, and B. S. N. Murthy. Functional validation of K-type (NiCr–NiMn) thin film thermocouple on low pressure turbine nozzle guide vane (LPT NGV) of gas turbine engine. *Experimental Techniques*, 41(2): 131–138, 2017. doi: 10.1007/s40799-016-0162-1.

[13] N. Klaas, R. Ottermann, F. Dencker, and M. C. Wurz. Development, characterisation and high-temperature suitability of thin-film strain gauges directly deposited with a new sputter coating system. *Sensors*, 20(11):3294, 2020. doi: 10.3390/s20113294.

[14] Y. Leng, F. Jones, and W. I. Milne. Characterization of Ni thin films following thermal oxidation in air. *Journal of Vacuum Science & Technology A*, 32(5):051402, 2014. doi: 10.1116/1.4895846.

[15] Ya. B. Losovyj et al. Oxidation mechanism of metallic chromium at room temperature. *Applied Surface Science*, 536:147842, 2021. doi: 10.1016/j.apsusc.2020.147842.

A Additional Figures

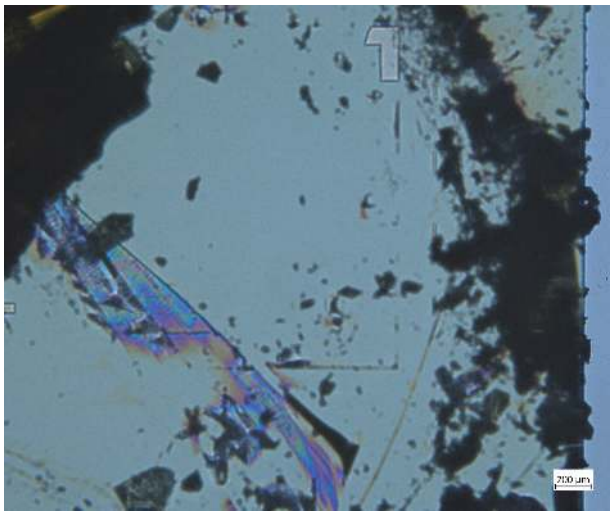

Figure 16: Optical micrograph of the donor chip following the first sugar liftoff attempt on sample variant A. Scale bar: 200 µm.

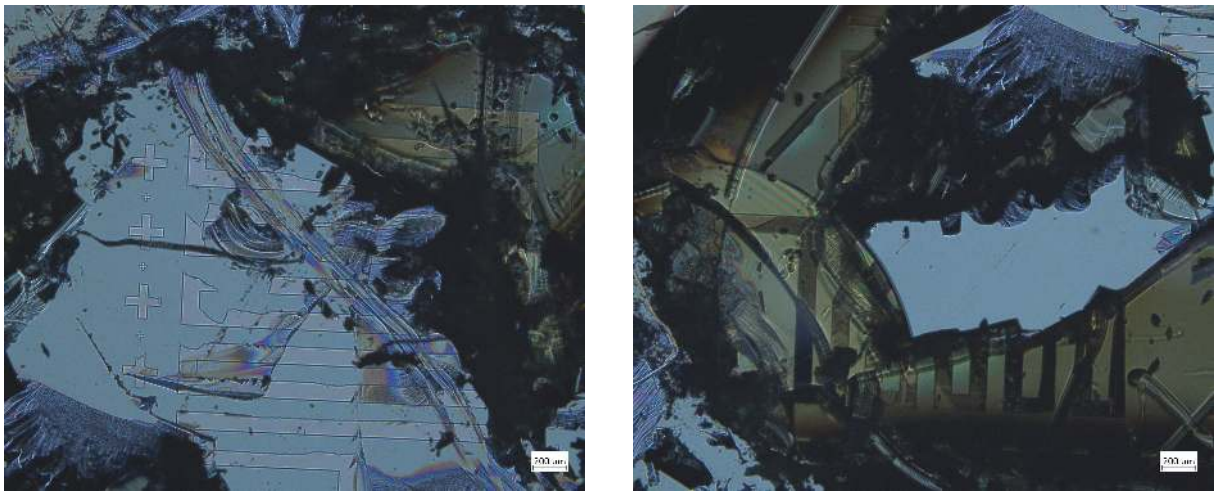

(a) (b)

Figure 17: Optical micrographs of the donor chip following liftoff of the thin sugar layer on sample variant A. Scale bars: 200 µm.

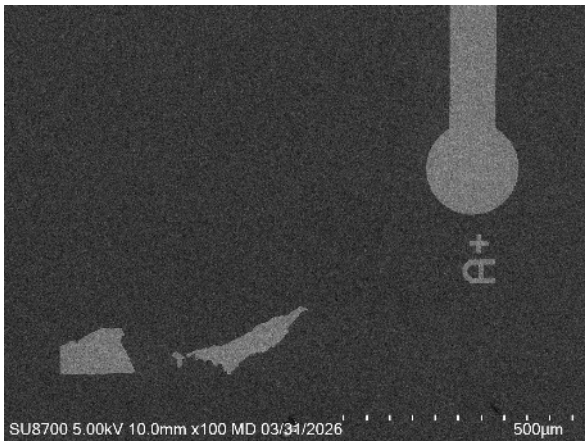

(a)

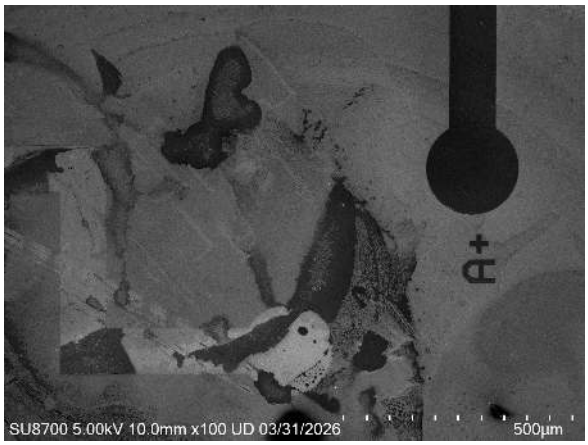

(b)

Figure 18: Additional SEM images of the donor chip following liftoff of the thin sugar layer on sample variant A. Scale bars: X µm.

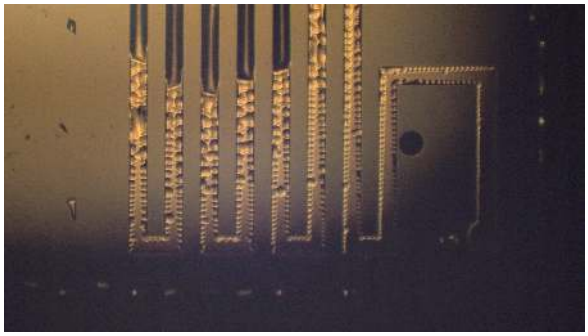

(a) Alumel (K−) pole region

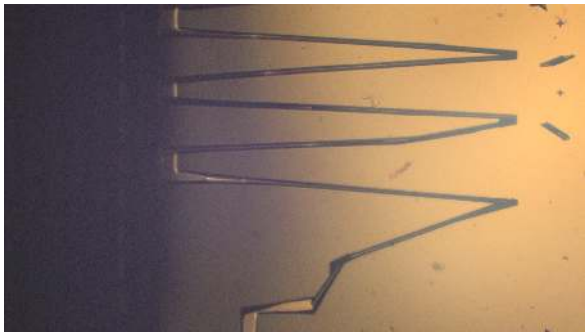

(b) Chromel (K+) pole region

(c) Alumel (K−) pole region

(d) Chromel (K+) pole region

Figure 19: Optical micrographs of the thin and thick sugar layer still in place on the sample variant B donor chip prior to liftoff. (a) shows the Alumel (K−) pole region of the thin sugar layer and (b) shows the Chromel (K+) pole region of the thin sugar layer. (c) shows the Alumel (K−) pole region of the thick sugar layer and (d) shows the Chromel (K+) pole region of the thick sugar layer.